

# Anisotropy, Itineracy, and Magnetic Frustration in High- $T_C$ Iron Pnictides

Myung Joon Han,\* Quan Yin\*, Warren E. Pickett, and Sergey Y. Savrasov  
Department of Physics, University of California, Davis, California 95616, USA  
(Dated: October 25, 2018)

Using first-principle density functional theory calculations combined with insight from a tight-binding representation, dynamical mean field theory, and linear response theory, we have extensively investigated the electronic structures and magnetic interactions of nine ferropnictides representing three different structural classes. The calculated magnetic interactions are found to be short-range, and the nearest ( $J_{1a}$ ) and next-nearest ( $J_2$ ) exchange constants follow the universal trend of  $J_{1a}/2J_2 \sim 1$ , despite their itinerant origin and extreme sensitivity to the z-position of As. These results bear on the discussion of itineracy versus magnetic frustration as the key factor in stabilizing the superconducting ground state. The calculated spin wave dispersions show strong magnetic anisotropy in the Fe plane, in contrast to cuprates.

Recent discovery of the new high-temperature superconductor,  $\text{LaO}_{1-x}\text{F}_x\text{FeAs}$  with a transition temperature ( $T_C$ ) of  $26\text{K}$  [1] has triggered tremendous research activities on iron pnictides. Rare-earth (*RE*) doping increases  $T_C$  up to  $55\text{K}$  for Sm [2, 3]. Replacing *RE-O* layers with Li produces an intrinsic superconductor  $\text{LiFeAs}$  with  $T_C$  of  $18\text{K}$  [4]. The 122 ferropnictides,  $\text{ALFe}_2\text{As}_2$  (*AL*: Ca, Sr, Ba, K), span another structural class with  $T_C$  up to  $38\text{K}$  [5, 6, 7, 8, 9, 10]. More recently, arsenic-free  $\text{FeSe}_{1-\delta}$  and  $\text{Fe}(\text{Se}_{1-x}\text{Te}_x)_{1-\delta}$  without any interlayer between Fe-(Se,Te) planes were found to be superconducting at  $T_C$  as high as  $27\text{K}$  under pressure [11, 12, 13, 14]. In spite of the accumulating reports of both experiments and theories, the nature of the superconductivity and magnetism is still far from clear. After several works have ruled out the electron-phonon coupling [15, 16], and the coexistence of magnetic fluctuation and superconductivity being confirmed by  $\mu\text{SR}$  [17], intensive investigations have been focused on the magnetic properties of these systems [18, 19, 20, 21, 22, 23, 24, 25]. From the studies up to now, one of the common and evident features is the interplay between superconductivity and magnetism. It is clear, from the different structures, that the essential physics lies in the iron plane forming the 2-dimensional spin lattice.

Except for the Fe(Se,Te) family suggested to have different magnetic structures by recent studies [18, 19, 20], it is widely believed that the first three classes of Fe pnictides have a common superconducting mechanism closely related to magnetic interactions. In order to clarify the raised issues and lead to further understanding, it is of key importance to investigate the exchange interactions across different classes of compounds and examine any trend or common features. However, material-specific information of magnetic interactions is scarce in spite of active research efforts. The direct probe of spin dynamics is inelastic neutron scattering, which has been recently performed for  $\text{SrFe}_2\text{As}_2$  [9] and  $\text{CaFe}_2\text{As}_2$  [26]. They have revealed that the combination of nearest and next nearest neighbor exchange interactions [ $J_{1a} + 2J_2$ ] is about  $100\text{meV}$ , but detailed data from individual con-

tributions, as well as their anisotropy and the proximity of the ratio  $J_{1a}/2J_2$  to unity, which has been discussed extensively in recent publications [21, 22, 23], are still missing.

In this Letter, using first-principle linear response calculations [27, 28], we provide the data of in-plane magnetic exchange couplings for several Fe-based superconductors, and discuss their spin wave dispersions. The data bear on the question of whether the values of exchange constants indicates magnetic fluctuations play an important role. A total of nine materials have been studied: *RE* FeAsO (*RE*: La, Ce, Pr, Nd),  $\text{ALFe}_2\text{As}_2$  (*AL*: Ca, Sr, Ba, K), and  $\text{LiFeAs}$ . Exchange interactions of these systems are found to be short-range despite the metallic density-of-states (DOS), and the calculated interaction strengths follow the universal behavior of  $J_{1a} \approx 2J_2$  for all materials, a relation that arises independently in the frustrated magnetic picture [21, 22, 23]. Considering not only the variety of the materials studied here but also the high sensitivity of the Fe moment to the z-position of As atom [29, 30], this universal behavior of the exchange interactions is impressive. The calculated spin-wave dispersion shows an anisotropic spin interaction which is different from the cuprates.

There have been several published tight-binding (TB) parametrizations of the electronic structure of prototypical  $\text{LaOFeAs}$  in the vicinity of the Fermi level using fits based either on Wannier functions or atomic basis sets [31, 32, 33, 34]. However the current situation still looks complicated because the projected DOS deduced from electronic structure calculations are based on the spherical harmonic projectors within the atomic spheres that may not be very well suited for the extended Fe and As orbitals presented here. Due to these complications even the crystal field splitting of Fe *d* level appears to be controversial in the current literature [31, 32, 33, 34].

To better understand the complicated electronic structure around Fermi level, we performed TB analysis by considering  $d_{xz}$  and  $d_{yz}$  orbitals of Fe  $t_{2g}$  manifold hybridizing with the arsenic  $p_x$  and  $p_y$ , respectively. As shown in Fig. 1, the separation between the energy levels

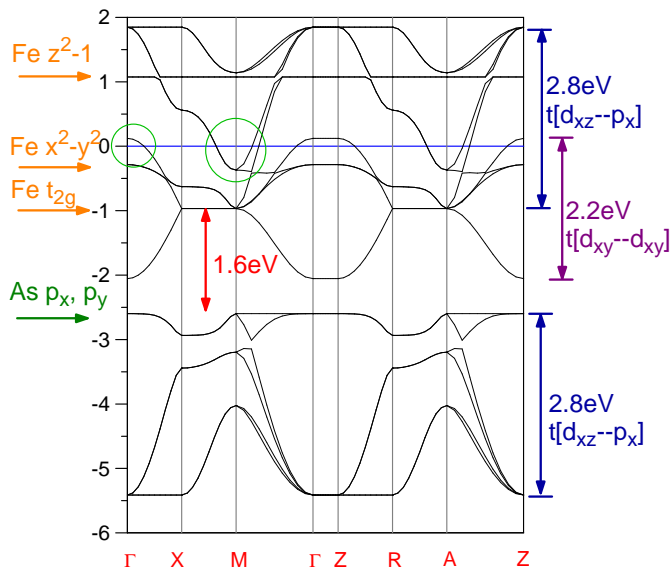


FIG. 1: (Color online) The tight-binding band structure of LaFeAsO. The circles at the Fermi level on the  $\Gamma$  and  $M$  points indicate the hole and electron pockets, respectively.

of Fe- $t_{2g}$  and As- $p_{x,y}$  states is about  $1.6eV$ . Accounting for the hybridization matrix element between  $d_{xz}-p_x$ ,  $d_{yz}-p_y$  states, which is of the order of  $1.8eV$ , produces bonding and antibonding bands, both having the bandwidth of  $2.8eV$  with the Fermi level falling into the antibonding part of the spectrum (approximately  $1eV$  above the Fe  $t_{2g}$  level). We also take into account the  $d_{xy}$  state of Fe which hybridizes with itself (hopping integral is approximately  $0.3eV$ ), which produces an additional bandwidth of  $2.2eV$ . The resulting bandwidth of Fe  $d$ -electron character near the Fermi level becomes  $2.8 + 2.2/2 = 3.9eV$  as exactly seen in the LDA calculation [35]. The coordinate system used for this TB description is the original crystallographic lattice where the spin alternates in the  $(\pi, \pi)$  direction. In this picture, the  $\Gamma$ -centered hole pockets (small circle in Fig. 1) are mostly of  $d_{xy}$  character, and the  $M$ -centered pockets (large circle) are of  $d_{xz}$ ,  $d_{yz}$  character. This picture can be fine-tuned further by including the  $d_{x^2-y^2}$  state which lies  $0.3eV$  below the Fermi level and hybridizes primarily with As- $p_{x,y}$  states (hopping integral is about  $0.8eV$ ) as well as hybridization between  $d_{xz,yz}$  orbitals with As  $p_z$  states (hopping integral is about  $0.4eV$ ). Note that in this picture the Fe  $d_{z^2-1}$  orbital becomes unoccupied and lies  $1eV$  above the Fermi level.

Now we discuss the exchange interactions. To calculate the interactions between Fe moments, we used linear response theory [36, 37] based on first-principle density functional theory (DFT) calculations, which has been successfully applied to the  $3d$  transition-metal oxides and the  $5f$  actinides metallic alloys [37, 38]. We used the full potential linearized muffin-tin orbital (LMTO) as

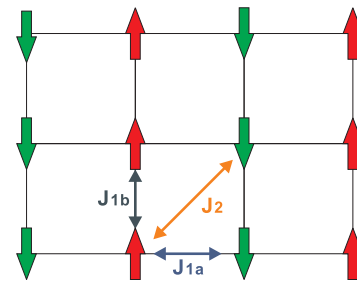


FIG. 2: (Color online) Spin arrangement and exchange interactions in the Fe plane of the striped  $Q_m$ -AFM phase. The arrows on lattice sites indicate the Fe spin directions.

the basis set [39] and local spin density approximation (LSDA) for the exchange-correlation (XC) energy functional. The LSDA is fairly good to describe the itinerant Fe  $3d$  states in these materials as shown in the previous studies and comparisons with angle resolved photoemission [29, 30, 35, 40]. In the calculations of REOFeAs compounds, we used the LSDA+DMFT method [27, 28] in which the RE  $4f$  orbitals are treated as the localized ones within Hubbard I approximation.  $U = 6eV$  and  $J_H = 0.86eV$  were used as the on-site Coulomb repulsion and Hund's rule exchange parameter. Lattice constants are taken from experiments, and we performed the calculations at various  $z(As)$ , including experimental  $z(As)_{exp}$  and LDA optimized  $z(As)_{LDA}$ .

Fig. 2 shows the spin structure of the Fe plane which is common to the all these materials. From here on we use the  $(\pi, 0)$  striped AFM coordinate system, which is convenient to discuss the spin wave dispersions. Magnetic interactions between Fe moments are governed by two dominating AFM couplings  $J_{1a}$  and  $J_2$ , and the FM nearest-neighbor exchange  $J_{1b}$  is small. We found the exchange couplings  $J(\mathbf{q})$  can be expressed in terms of short-range exchange constants. This character suggests pursuing a comparison with local moment models with AFM spin interactions[21, 22, 23]. The short range couplings do not conflict with the itinerant magnet picture because although the Fe  $3d$  orbital has finite DOS at the Fermi level, the magnetic interactions can still remain short range, which possibly reflects the bad metallicity and some correlation effects.

The calculated Fe magnetic moments and exchange interactions are summarized in Table I. We use the convention that positive  $J$  means AFM couplings. The calculated moments are consistent throughout the materials. The calculations done at experimental  $z(As)_{exp}$  are known to predict the moments about twice as large as experimental values, while at optimized  $z(As)_{LDA}$  they give smaller moments. The cases in which DFT overestimates magnetic moments are rare, and the cause is still under debate for Fe oxyphnictides. Although some theorists suggest it is due to the frustrated magnetic struc-

System	Moment	$J_{1a}$	$J_2$	$J_{1b}$	$J_{1a}/2J_2$	$J_{1a} + 2J_2$
LaFeAsO	1.69	47.4	22.4	-6.9	1.06	92.2
CeFeAsO	1.79	31.6	15.4	2.0	1.03	62.4
PrFeAsO	1.76	57.2	18.2	3.4	1.57	93.6
NdFeAsO	1.49	42.1	15.2	-1.7	1.38	72.5
CaFe <sub>2</sub> As <sub>2</sub>	1.51	36.6	19.4	-2.8	0.95	75.4
SrFe <sub>2</sub> As <sub>2</sub>	1.69	42.0	16.0	2.6	1.31	74.0
BaFe <sub>2</sub> As <sub>2</sub>	1.68	43.0	14.3	-3.1	1.51	71.5
KFe <sub>2</sub> As <sub>2</sub>	1.58	42.5	15.0	-2.9	1.42	72.5
LiFeAs	1.69	43.4	22.9	-2.5	0.95	89.2

TABLE I: Calculated Fe moments (in  $\mu_B$ ) and in-plane exchange interactions (in  $meV$ ), using experimental  $z(As)$ .

ture [21], Mazin and Johannes suggest an alternative picture [41] based on magnetic fluctuation and inhomogeneities. Importantly, the electronic structure features such as electron-hole symmetry and the exchange interaction strengths are better described with  $z(As)_{exp}$  when compared to available experimental data [9, 26]. Thus our discussion will be based on the results from  $z(As)_{exp}$ . The sensitivity of moments and exchange interactions to  $z(As)$  is large. For example, in LaFeAsO the change of  $z(As)$  by  $0.04\text{\AA}$  ( $\Delta z(As) = 0.005$  in terms of internal coordinates) induces about 10% difference in the moment and up to 20% in the exchange interactions [29]. The same order of sensitivity was also reported for CaFe<sub>2</sub>As<sub>2</sub> [30]. Therefore the deviation of up to 8% for moments and 30% for major exchange interactions ( $J_{1a}$  and  $J_2$ ) are not significant, and become much smaller if  $z(As)$  could be refined for each material. Taking this into account, we can say that the magnetic moments and exchange interactions are uniform throughout the materials considered here.

One of the most important quantities to understand the magnetism and possibly the superconducting mechanism in these materials is the ratio of  $J_{1a}/2J_2$ , which has so far not been measured nor calculated. According to the spin Hamiltonian models [21, 22, 23], assuming Fe pnictides as magnetic Mott insulators like cuprates, at  $J_{1a}/2J_2 \approx 1$  the system is close to the quantum critical regime, so a superconducting ground state may appear as a result of the magnetic fluctuation [21, 22, 23, 42]. Note that the calculated ratios shown in Table I are all around unity, demonstrating that this universal behavior of  $J_{1a}/2J_2$  can arise from itinerant magnetism, without the system being close to a Mott transition. The deviations of  $J_{1a}/2J_2$  from unity reflect not only the intrinsic material properties but also the sensitive dependence on  $z(As)$ . Although there is no apparent relation between the  $J_{1a}/2J_2$  ratio and  $T_C$ , the universal feature of  $J_{1a}/2J_2$  near unity is closely associated to superconductivity since it is present throughout the materials studied here. The connection between itinerant AFM and super-

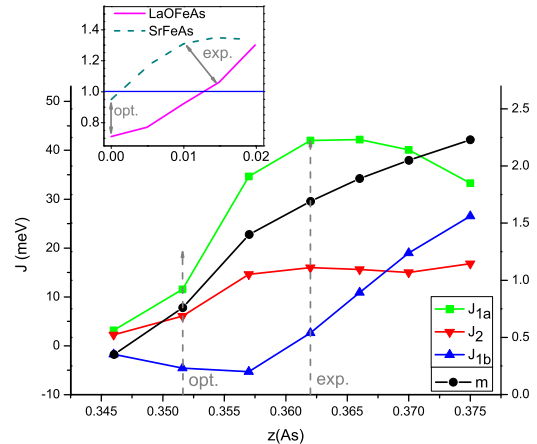


FIG. 3: value (exp.) and theoretically optimized value (opt.) of  $z(As)$ . In the inset figure, the LDA-optimized  $z(As)$  is set to be zero reference.

conductivity has been discussed previously [43].

Another important quantity is  $|J_{1a} + 2J_2|$  which determines the spin wave velocity in the  $(\pi, 0)$  direction, and can be directly probed by neutron scattering experiments. The available experimental data are in general agreement with our calculation. For SrFe<sub>2</sub>As<sub>2</sub> calculation shows  $|J_{1a} + 2J_2| = 74meV$ , not much smaller than the  $100 \pm 20meV$  measured by neutron scattering [9]. Also, for CaFe<sub>2</sub>As<sub>2</sub> our calculated  $|J_{1a} + 2J_2| = 75meV$  is slightly smaller than the measured  $95 \pm 16meV$  [26] (derived from the observed spin wave velocity, see eq.(2) below). Especially our result for BaFe<sub>2</sub>As<sub>2</sub> is in good agreement with recent experiment by Ewings *et al.* [44]: One of their best fits shows that  $J_{1a} = 36meV$ ,  $J_2 = 18meV$ , and  $J_{1b} = -7meV$ .

As an example, Fig. 3 shows the  $z(As)$ -dependence of the magnetic moments and interactions of SrFe<sub>2</sub>As<sub>2</sub>. The moment is a simple monotonic function of  $z(As)$  ranging from  $0.35\mu_B$  to  $2.23\mu_B$ . The three  $J$ 's have different behaviors.  $J_{1a}$  increases rapidly with  $z(As)$  at the beginning, saturates in the middle, and eventually turns down. This behavior is a result of the hybridization between Fe  $d_{xz,yz}$  and As  $p_{x,y}$  orbitals, as we discussed in the tight-binding representation. Due to the shape and orientation of the Fe  $d_{xz,yz}$  and As  $p_{x,y}$  orbitals, there is a certain  $z(As)$  that gives the maximum overlapping, and hence largest  $J_{1a}$ . Note that  $J_{1b}$  changes sign at  $z(As)_{exp}$ , and eventually surpasses  $J_2$ . Also,  $J_{1a}$  and  $J_2$  plateau in the small region around  $z(As)_{exp}$ . Similar behaviors are also found in other materials. The  $J_{1a}/2J_2$  and  $|J_{1a} + 2J_2|$  values presented in Table I are robust against the small deviations in  $z(As)$  around the experimental values. From the data one can also calculate  $J_{1a}/2J_2$  vs.  $z(As)$ , which reveals the existence of

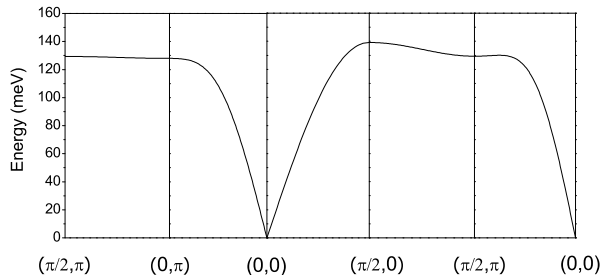


FIG. 4: The calculated spin wave dispersion of  $\text{SrFe}_2\text{As}_2$  along high-symmetry lines, the exchange constants are given in Table I.

the “sweet spot” where the optimal ratio  $J_{1a}/2J_2 = 1$  is achieved independent of any Heisenberg model assumption. In the case of  $\text{SrFe}_2\text{As}_2$  it is  $z(\text{As}) = 0.357$  (the inset of Fig. 3).

The calculated spin wave dispersion gives more intuitive information about the magnetic interaction and anisotropy of these systems [9, 25]. The dispersion relation of the 2D striped-AFM lattice reads

$$\omega(\mathbf{q}) = S\sqrt{(\mathcal{J}_0 + J_{1b}(\mathbf{q}))^2 - (J_{1a}(\mathbf{q}) + J_2(\mathbf{q}))^2}. \quad (1)$$

Using the calculated magnetic exchange constants, we plot the spin wave dispersion of  $\text{SrFe}_2\text{As}_2$  in Fig. 4, whose  $S = 0.94$  is taken from experiment [8]. The non-symmetric dispersions in  $(0, 0) - (0, \pi)$  and  $(0, 0) - (\pi, 0)$  directions indicate in-plane magnetic anisotropy, which is a major difference from cuprates. At small  $q$  near  $(0, 0)$ , the spin wave velocity in the  $(\pi, 0)$  direction is

$$v_{\perp} = 2aS|J_{1a} + 2J_2|, \quad (2)$$

which is the relation used to experimentally determine  $|J_{1a} + 2J_2|$ , such as for  $\text{SrFe}_2\text{As}_2$  [9]. The difference in  $J_{1a}$  and  $J_{1b}$ , a direct consequence of the  $Q_M$ -AFM ordering that breaks in-plane symmetry, accounts for the anisotropy in  $(\pi, 0)$  and  $(0, \pi)$  directions. These anisotropic spin waves can be directly probed by neutron scattering experiments on single crystals.

To conclude, we have studied magnetic exchange interactions in various Fe-based high  $T_C$  superconductors using first-principle based linear response calculations. From the nine different materials, the magnetic interactions are short-range and can be well described by the first and second nearest-neighbor interactions. Importantly  $J_1/2J_2$  is close to unity for all the cases, just as would be the case for the frustration limit of a local moment model. Calculated spin wave dispersions show the magnetic anisotropy and the roles of the three in-plane exchange interactions. Our result strongly suggests the magnetic fluctuation as the pairing mechanism for the superconducting ground state.

The authors would like to thank Elihu Abrahams (Rutgers Univ.) and Rajiv Singh (UC Davis) for helpful discussions on the spin wave dispersion. The authors acknowledge support from NSF Grants DMR-0606498 (S.Y.S) and DMR-0421810 (W.E.P), and collaborative work supported by DOE SciDAC Grants SE-FC0206ER25793 and DE-FC02-06ER25794.

\* These authors have contributed equally to this paper.

- [1] Y. Kamihara *et al.*, J. Am. Chem. Soc. **130**, 3296 (2008).
- [2] X. H. Chen *et al.*, Nature **453**, 761 (2008).
- [3] Z. A. Ren *et al.*, Chinese Phys. Lett. **25**, 2215 (2008).
- [4] J. H. Tapp *et al.*, Phys. Rev. B **78**, 060505(R) (2008).
- [5] C. Krellner *et al.*, Phys. Rev. B **78**, 100504(R) (2008).
- [6] A. Jesche *et al.*, arXiv:0807.0632 (2008).
- [7] A. I. Goldman *et al.*, Phys. Rev. B **78**, 100506(R) (2008).
- [8] J. Zhao *et al.*, Phys. Rev. B **78**, 140504(R) (2008).
- [9] J. Zhao *et al.*, Phys. Rev. Lett. **101**, 167203 (2008).
- [10] L. Zhao *et al.*, arXiv:0807.0398 (2008).
- [11] F. -C. Hsu *et al.*, PNAS **105**, 14262 (2008).
- [12] M. H. Fang *et al.*, Phys. Rev. B **78**, 224503 (2008).
- [13] K. -W. Yeh *et al.*, Europhysics Lett. **84**, 37002 (2008).
- [14] Y. Mizuguchi *et al.*, Appl. Phys. Lett. **93**, 152505 (2008).
- [15] L. Boeri, O. V. Dolgov and A. A. Golubov, Phys. Rev. Lett. **101**, 026403 (2008).
- [16] K. Huale, J. H. Shim and G. Kotliar, Phys. Rev. Lett. **100**, 226402 (2008).
- [17] A. J. Drew *et al.*, Phys. Rev. Lett. **101**, 097010 (2008).
- [18] W. Bao *et al.*, arXiv:0809.2058 (2008).
- [19] J. J. Pulikotil, M. van Schilfhaarde, and V. P. Antropov, arXiv:0809.0283 (2008).
- [20] F. Ma *et al.*, arXiv:0809.4732 (2008).
- [21] Q. Si and E. Abrahams, Phys. Rev. Lett. **101**, 076401 (2008).
- [22] C. Fang *et al.*, Phys. Rev. B **77**, 224509 (2008).
- [23] C. Xu, M. Müller, and S. Sachdev, Phys. Rev. B **78**, 020501 (2008).
- [24] J. Wu, P. Phillips, and A. H. Castro Neto, Phys. Rev. Lett. **101**, 126401 (2008).
- [25] G. S. Uhrig *et al.*, arXiv:0810.3068 (2008).
- [26] R. J. McQueeney *et al.*, Phys. Rev. Lett. **101**, 227205 (2008).
- [27] A. Georges *et al.*, Rev. Mod. Phys. **68**, 13 (1996).
- [28] G. Kotliar *et al.*, Rev. Mod. Phys. **78**, 865 (2006).
- [29] Z. P. Yin *et al.*, Phys. Rev. Lett. **101**, 047001 (2008).
- [30] T. Yildirim, Phys. Rev. Lett. **101**, 057010 (2008).
- [31] K. Kuroki *et al.*, Phys. Rev. Lett. **101**, 087004 (2008).
- [32] C. Cao, P. J. Hirschfeld, and H.-P. Cheng, Phys. Rev. B **77**, 220506 (2008).
- [33] K. Nakamura, R. Arita, and M. Imada, J. Phys. Soc. Jpn. **77**, 093711 (2008).
- [34] E. Manousakis *et al.*, arXiv:0806.3432 (2008).
- [35] D. J. Singh and M.-H. Du, Phys. Rev. Lett. **100**, 237003 (2008).
- [36] A. I. Liechtenstein *et al.*, J. Magn. Magn. Mater. **67**, 65 (1987); P. Bruno, Phys. Rev. Lett. **90**, 087205 (2003).
- [37] X. Wan, Q. Yin, and S. Y. Savrasov, Phys. Rev. Lett. **97**, 266403 (2006).
- [38] M. J. Han, X. Wan, and S. Y. Savrasov, Phys. Rev. B

- 78**, 060401 (R) (2008).
- [39] S. Y. Savrasov, Phys. Rev. B **54**, 16470 (1996).
- [40] D. H. Lu *et al.*, Nature **455**, 81 (2008).
- [41] I. I. Mazin and M. D. Johannes, Nature Physics doi:10.1038/nphys1160 (2008).
- [42] A. V. Chubukov, D. Efremov and I. Eremin, Phys. Rev. B **78**, 134512 (2008).
- [43] T. Moriya, Proc. Jpn. Acad. Ser. B **82**, 1 (2006).
- [44] R. A. Ewings *et al.*, Phys. Rev. B **78**, 220501 (R) (2008).
- [45] Where  $J_{1a}(\mathbf{q}) = 2J_{1a} \cos q_x$ ,  $J_2(\mathbf{q}) = 2J_2[\cos(q_x + q_y) + \cos(q_x - q_y)]$ ,  $J_{1b}(\mathbf{q}) = 2J_{1b} \cos q_y$ , and  $\mathcal{J}_0 = 2J_{1a} + 4J_2 - 2J_{1b}$ .